High Temperature Superconductivity (HTSC)

PROGRESS IN SUPERCONDUCTIVITY

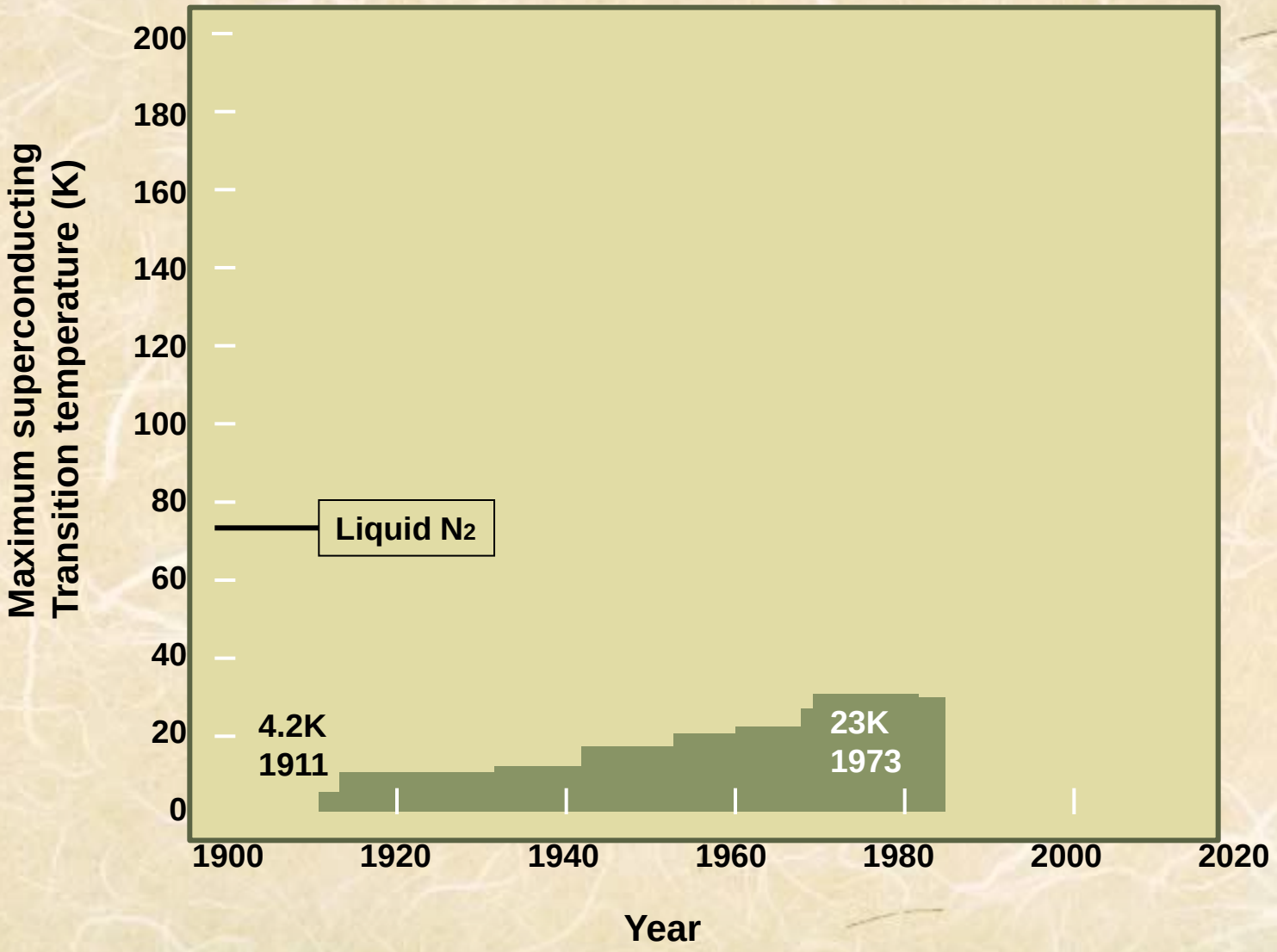

PROGRESS IN SUPERCONDUCTIVITY

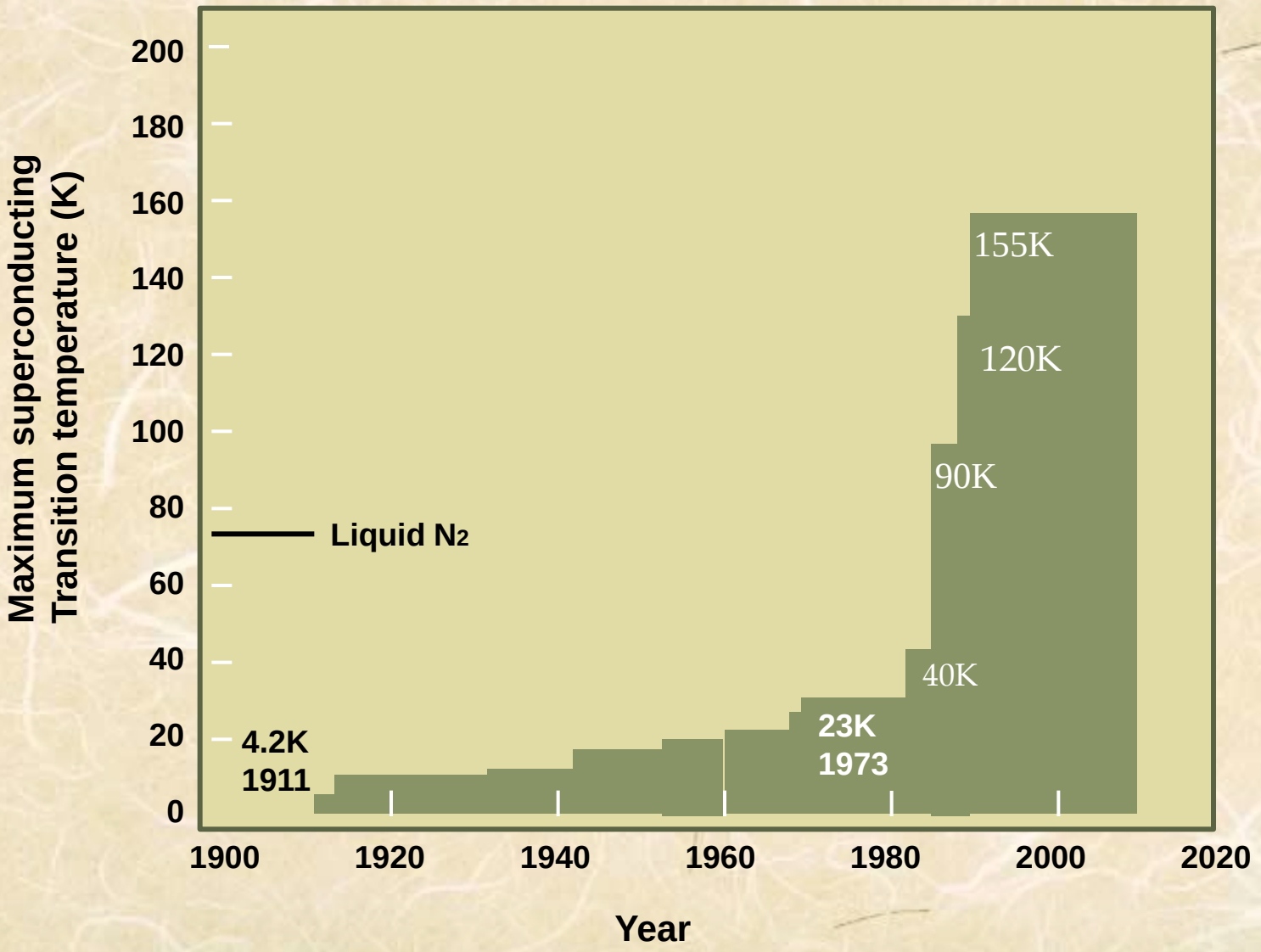

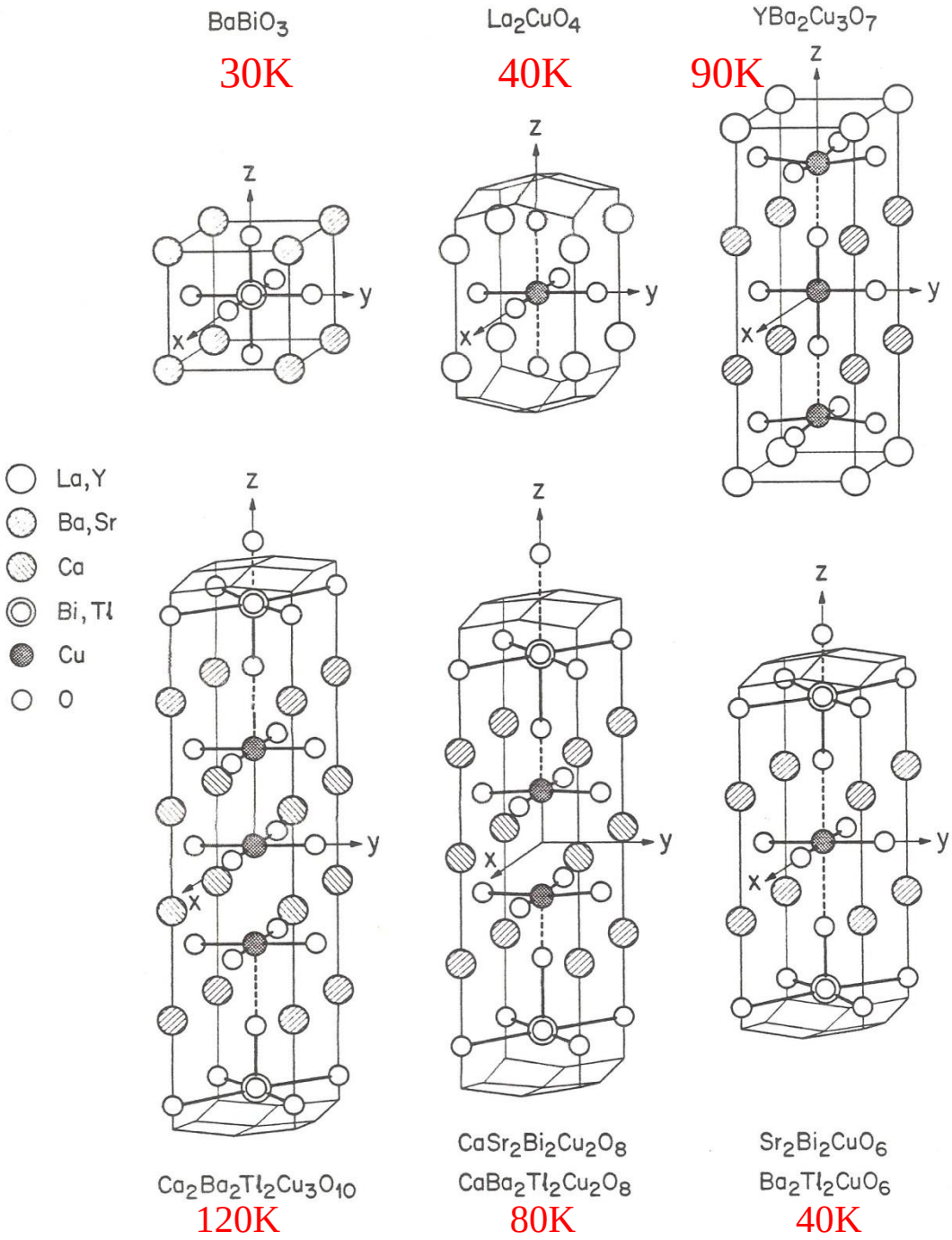
BaBiO3
30K
La2CuO4
40K
YBa2Cu3O7
90K
La,Y
Ba,Sr
Ca
Bi,Tl
Cu
O
Ca2Ba2Tl2Cu3O10
120K
CaSr2Bi2Cu2O8
CaBa2Tl2Cu2O8
80K
Sr2Bi2CuO6
Ba2Tl2CuO6
40K

High Temperature Superconductor $YBa_2Cu_3O_7$

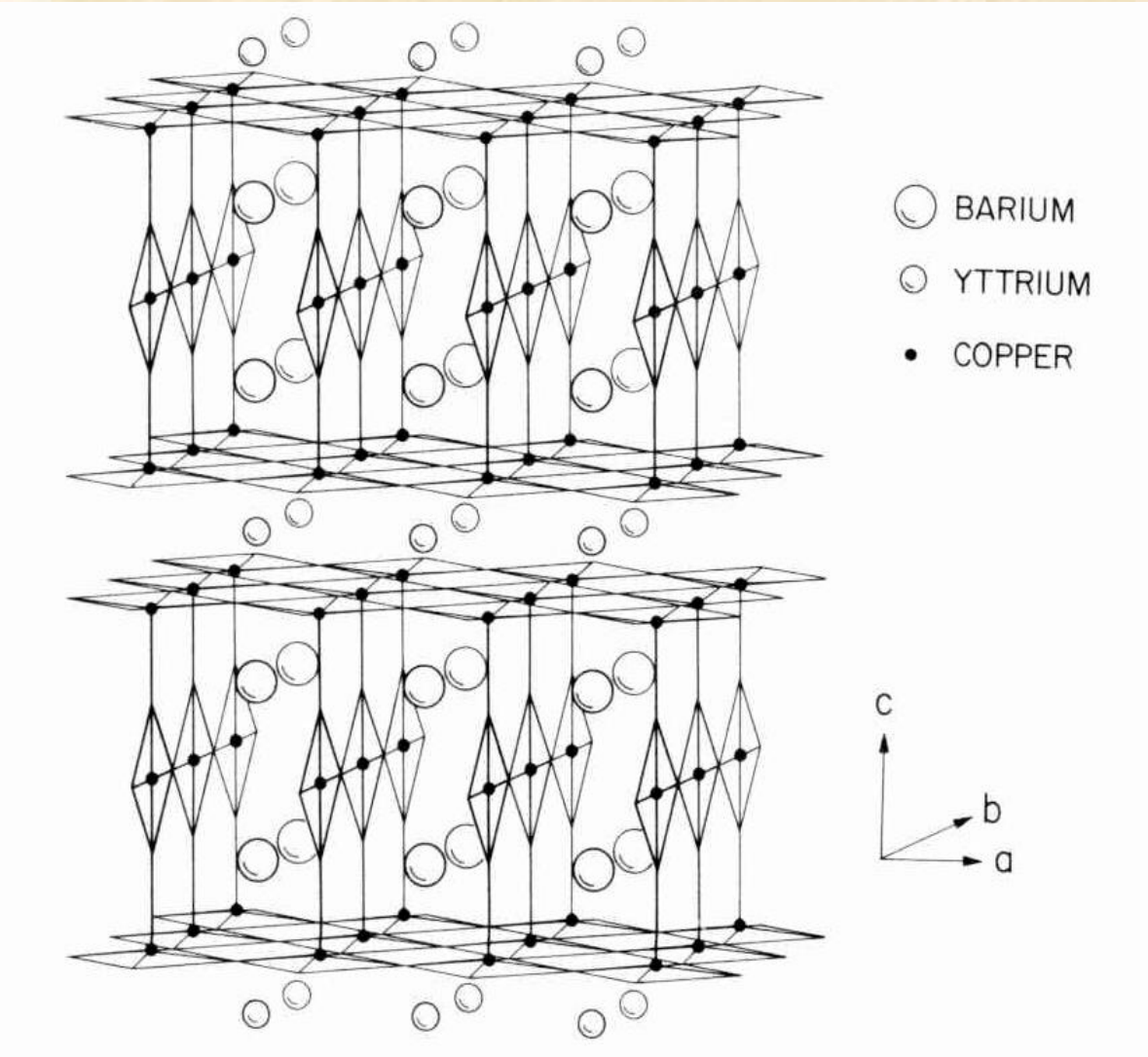

Invention of Oxide Molecular Beam Epitaxy in 1988 For HTSC Single Crystal Films.

La_2CuO_4 Structure,
with Ba doping on La site, T_c = 32K (8/1986)
with Sr doping on La site, T_c = 40K (12/1986)

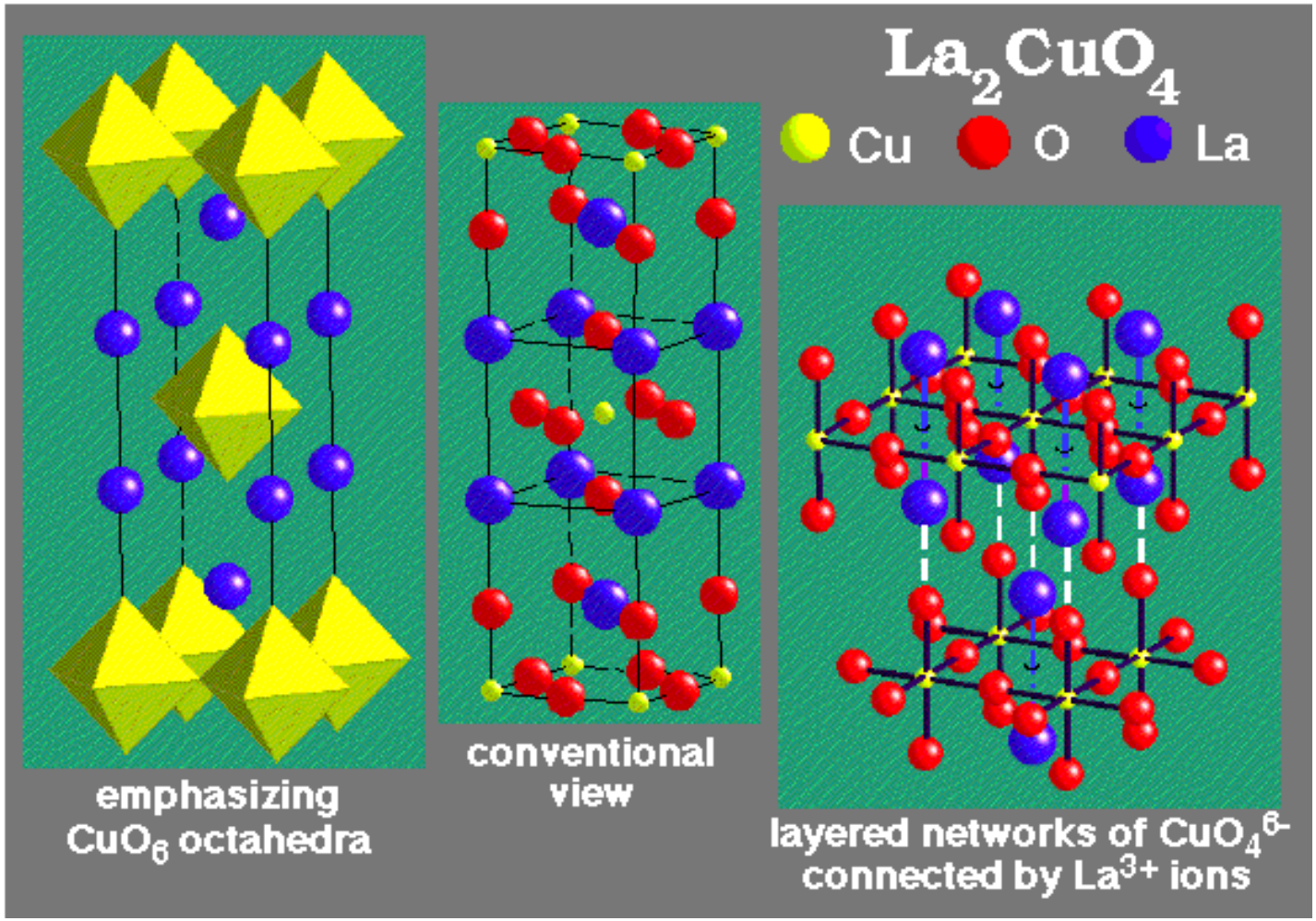

$Y_1Ba_2Cu_3O_{7-x}$ Structure, with T_c = 90K (1987)

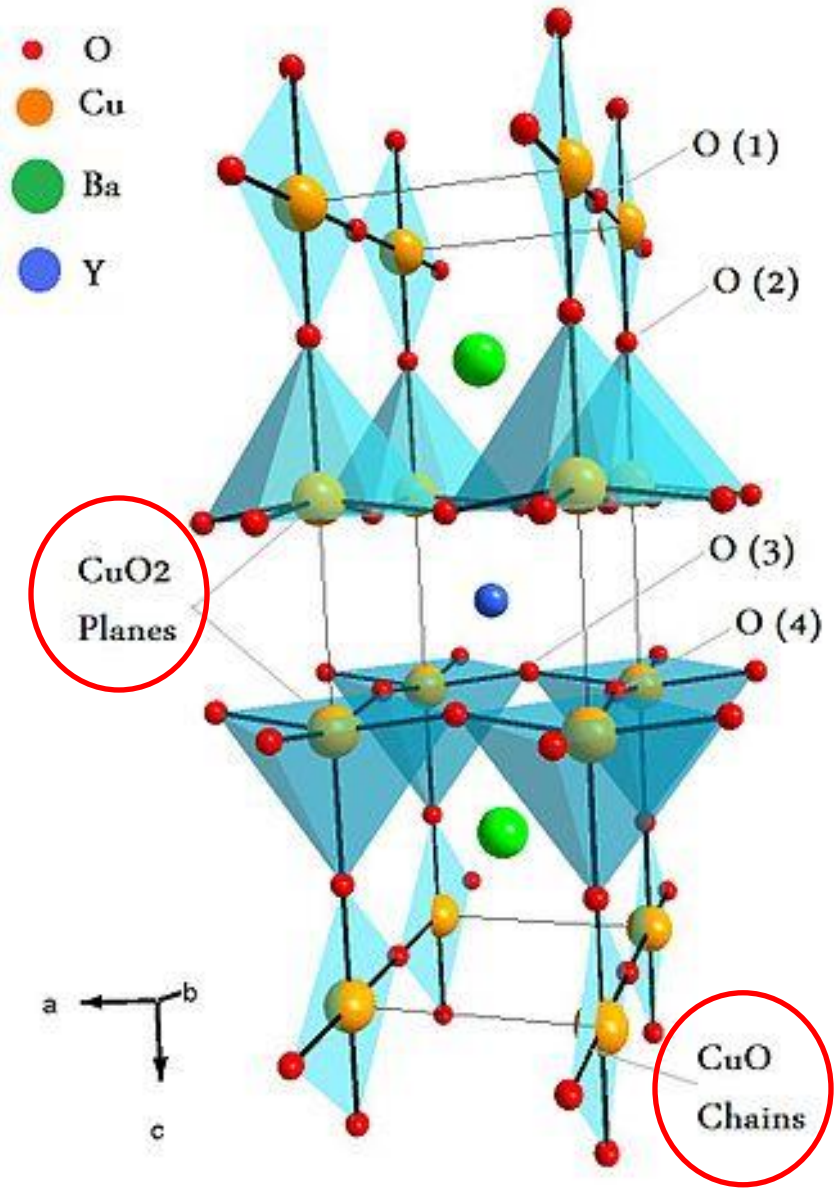

- One of the key feature of the unit cell of $YBa_2Cu_3O_{7-x}$ is the presence of **two layers of CuO_2.**
- The role of the Y plane is to serve as a spacer between two CuO_2 planes. In YBCO, **the Cu–O chains** are known to play an important role for superconductivity.
- T_c is maximal near 92 K when $x \approx 0.15$ and the structure is orthorhombic.
- Superconductivity disappears at $x \approx 0.6$, where the structural transformation of YBCO occurs from orthorhombic to tetragonal.

Crystal structures of high-temperature ceramic superconductors

- The structure of high-T_c copper oxide or cuprate superconductors are often closely related to **perovskite** structure, and the structure of these compounds has been described as a distorted, oxygen deficient multi-layered perovskite structure.
- One of common features of the crystal structure of oxide superconductors is an alternating multi-layer of CuO_2 planes with superconductivity taking place between these layers. The more layers of CuO_2 , the higher T_c.
- This structure causes a large *anisotropy* in normal conducting and superconducting properties, since electrical currents are carried by **holes induced in the oxygen sites of the CuO_2 sheets**. The electrical conduction is highly anisotropic, with a much higher conductivity parallel to the CuO_2 plane than in the perpendicular direction.
- Generally, Critical temperatures depend on the chemical compositions, cations substitutions and oxygen content.

$Y_1Ba_2Cu_3O_{7-x}$ Structure

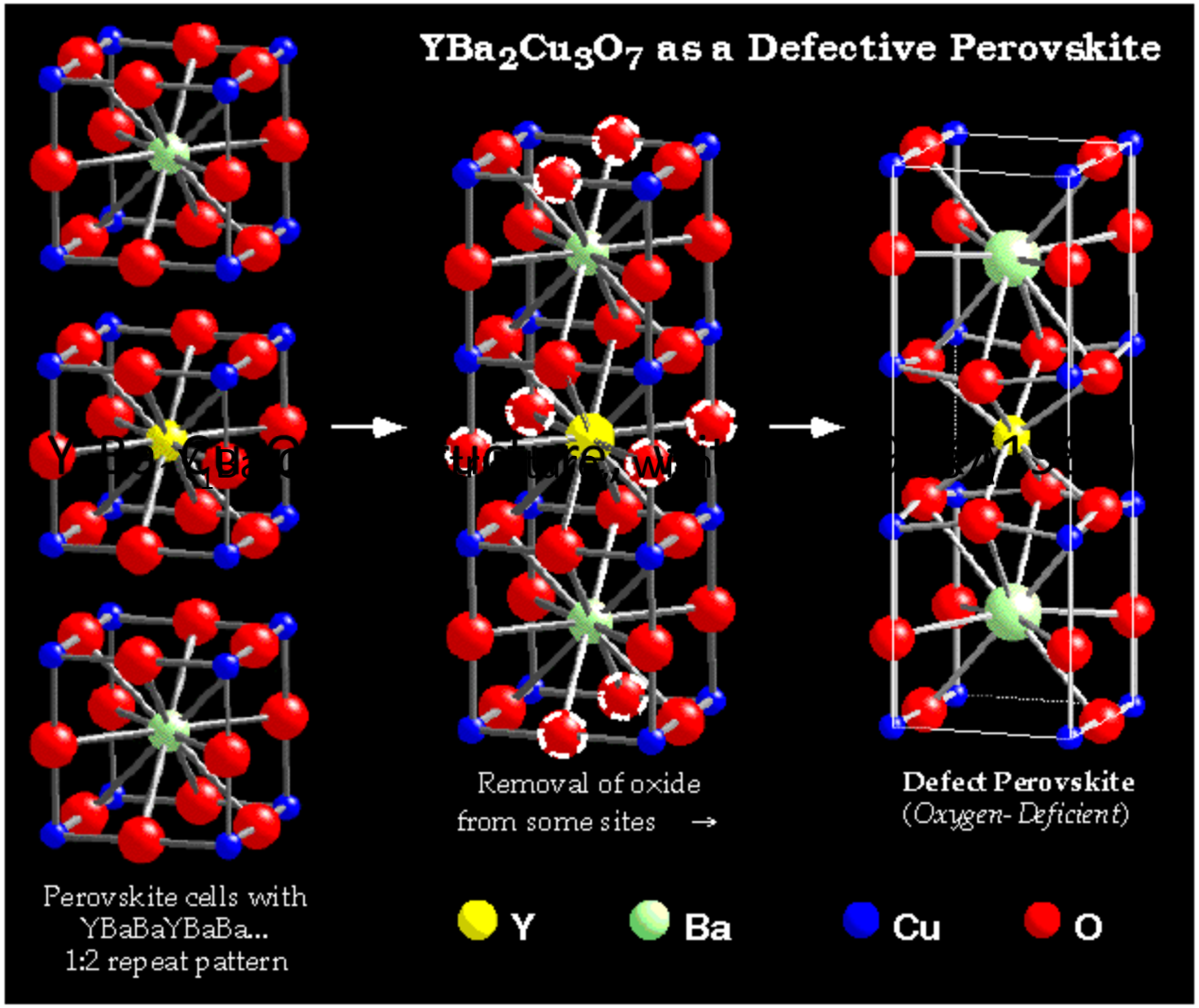

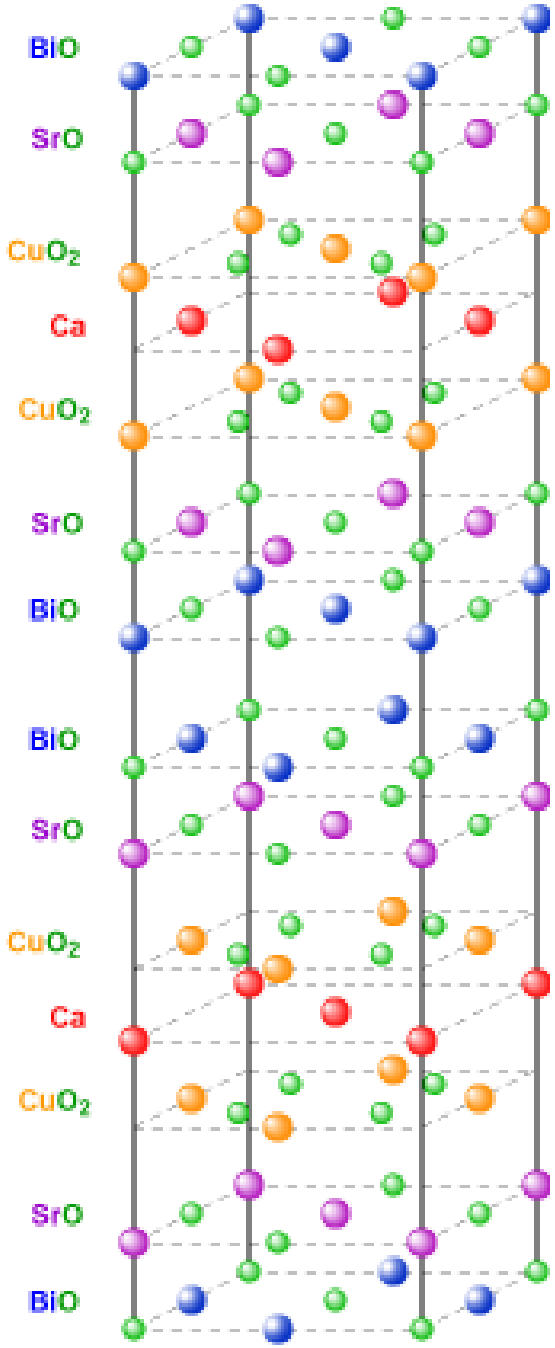

$Bi_2Sr_2Ca_{n-1}Cu_nO_{2n+4+x}$, n =1, 2, 3
T_c of 80K (n =2), and 122K (n =3)

- The crystallographic unit cell of BSCCO-2212 comprising two repeat units offset by (1/2,0,0).
- The other BSCCO family members have very similar structures: 2201 has one less CuO_2 in its top and bottom half and no Ca layer,
- while 2223 has an extra CuO_2 and Ca layer in each half

A small sample of the high-temperature superconductor BSCCO-2223

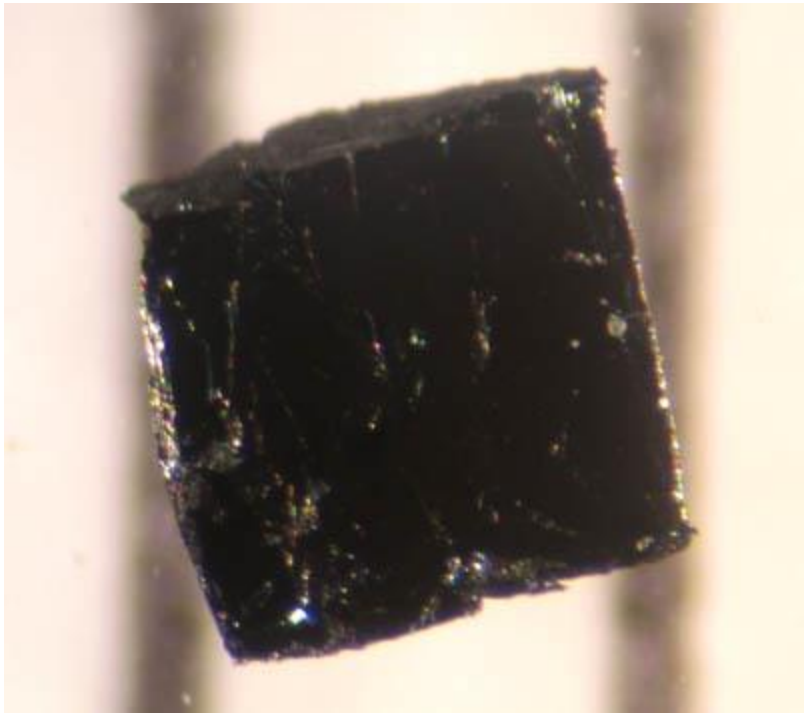

$Tl_1Ba_2Ca_nCu_{n+1}O_{7-x}$, with n = 0, 1, 2, 3

$Tl_2Ba_2Ca_nCu_{n+1}O_{7-x}$, with n = 0, 1, 2

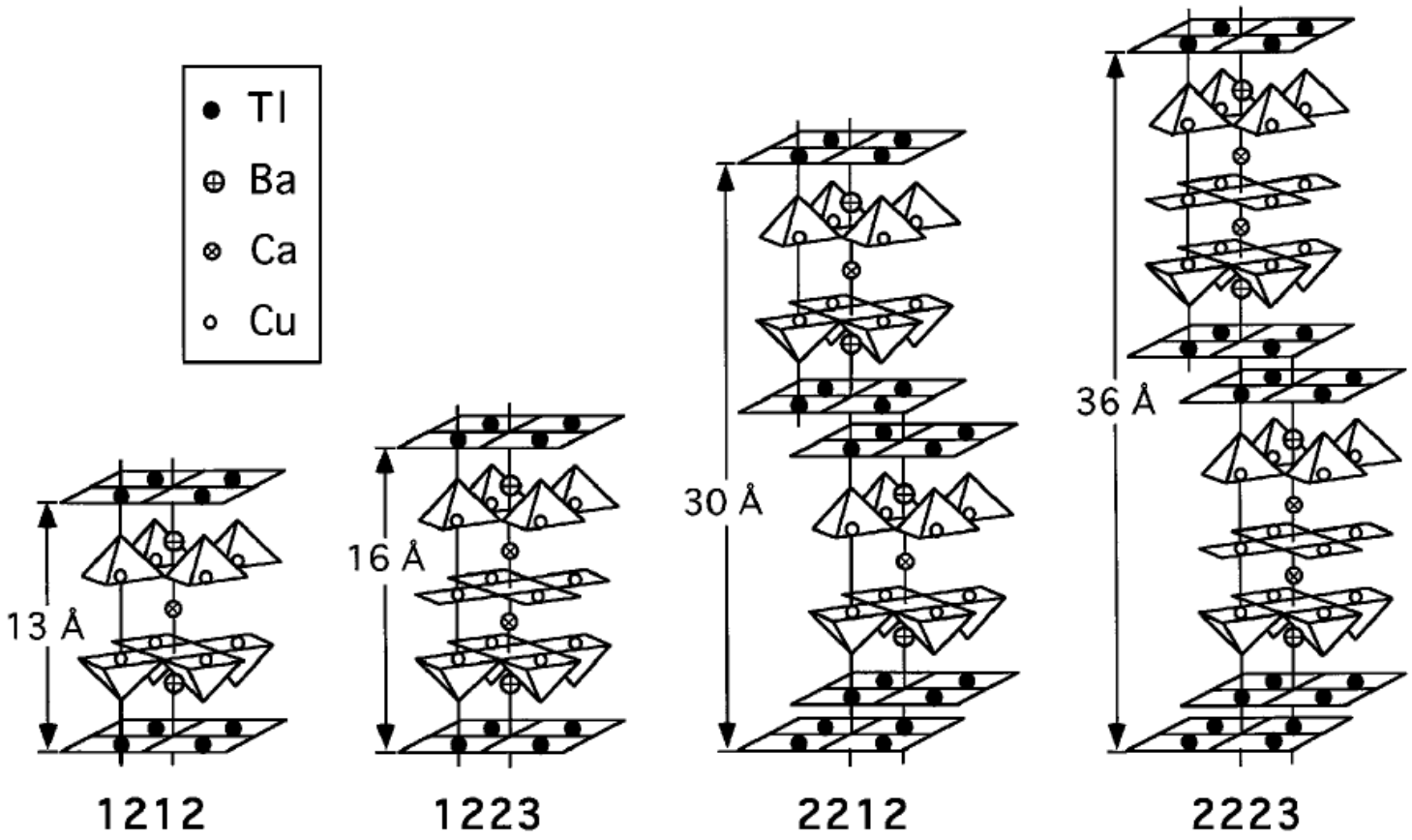

FIG. 1. Depictions of the Tl-1212, Tl-1223, Tl-2212, and Tl-2223 crystal structures.

T_c = 108K T_c= 125K

Hg–Ba–Ca–Cu–O superconductor:

- The crystal structure of $HgBa_2CuO_4$ (Hg-1201), $HgBa_2CaCu_2O_6$ (Hg-1212) and $HgBa_2Ca_2Cu_3O_8$ (Hg-1223) is similar to that of Tl-1201, Tl-1212 and Tl-1223, with Hg in place of Tl.
- It is noteworthy that the T_c of the Hg compound (Hg-1201) containing one CuO_2 layer is much larger as compared to the one-CuO_2-layer compound of thallium (Tl-1201).
- In the Hg-based superconductor, T_c is also found to increase as the CuO_2 layer increases. For Hg-1201, Hg-1212 and Hg-1223, the values of T_c are 94, 128 and the record value at ambient pressure 134 K.
- The observation that the T_c of Hg-1223 increases to 153 K under high pressure indicates that the T_c of this compound is very sensitive to the structure of the compound.

Critical temperature (T_c), crystal structure, and lattice constants of Representative high-T_c superconductors

Critical temperature (Tc), crystal structure and lattice constants of some high-Tc superconductors

Formula	Notation	T_c (K)	No. of Cu-O planes in unit cell	Crystal structure
$YBa_2Cu_3O_7$	123	92	2	Orthorhombic
$Bi_2Sr_2CuO_6$	Bi-2201	20	1	Tetragonal
$Bi_2Sr_2CaCu_2O_8$	Bi-2212	85	2	Tetragonal
$Bi_2Sr_2Ca_2Cu_3O_6$	Bi-2223	110	3	Tetragonal
$Tl_2Ba_2CuO_6$	Tl-2201	80	1	Tetragonal
$Tl_2Ba_2CaCu_2O_8$	Tl-2212	108	2	Tetragonal
$Tl_2Ba_2Ca_2Cu_3O_{10}$	Tl-2223	125	3	Tetragonal
$TlBa_2Ca_3Cu_4O_{11}$	Tl-1234	122	4	Tetragonal
$HgBa_2CuO_4$	Hg-1201	94	1	Tetragonal
$HgBa_2CaCu_2O_6$	Hg-1212	128	2	Tetragonal
$HgBa_2Ca_2Cu_3O_8$	Hg-1223	134	3	Tetragonal

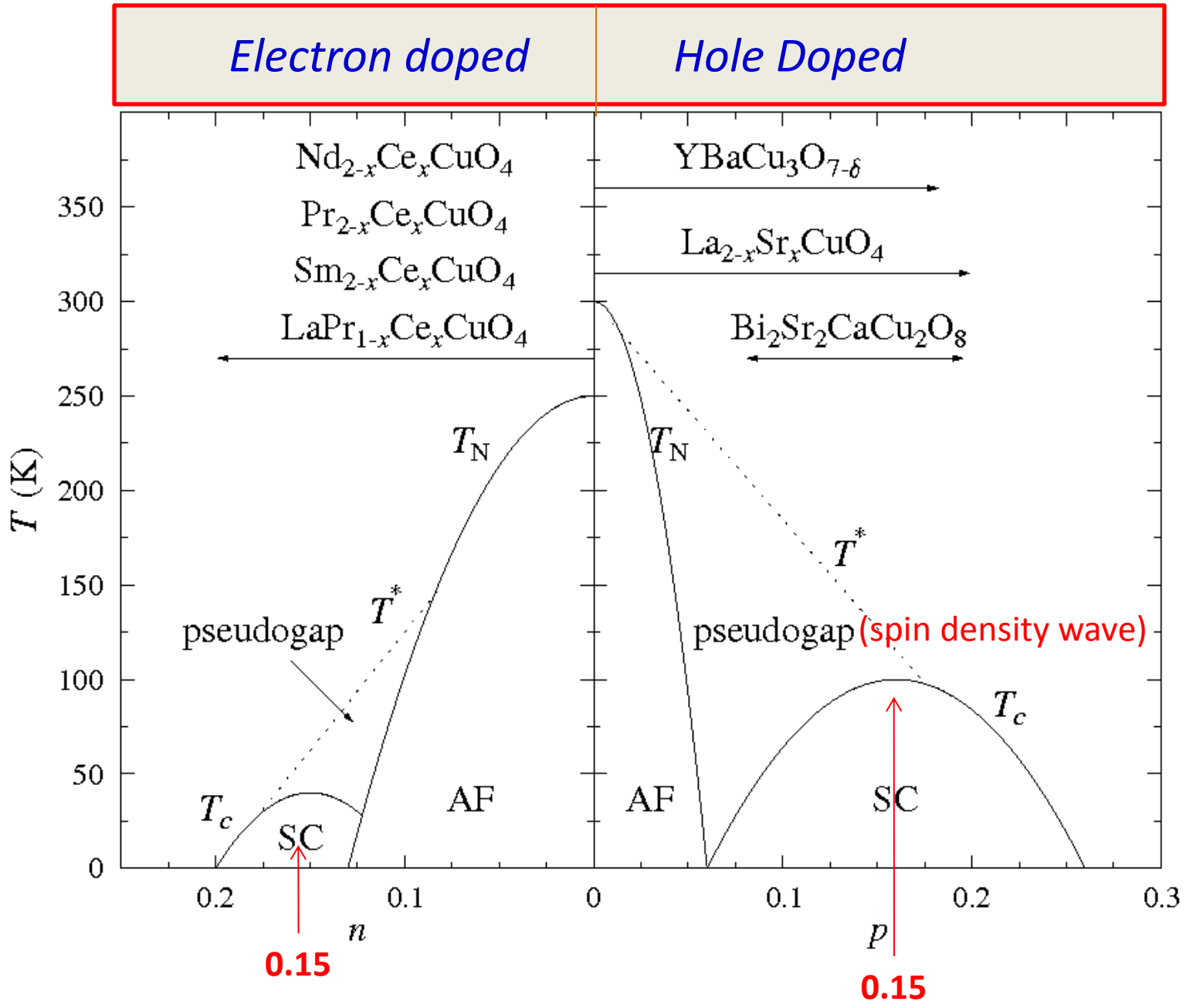
Electron doped
Hole Doped
$Nd_{2-x}Ce_xCuO_4$
$Pr_{2-x}Ce_xCuO_4$
$Sm_{2-x}Ce_xCuO_4$
$LaPr_{1-x}Ce_xCuO_4$
$YBaCu_3O_{7-\delta}$
$La_{2-x}Sr_xCuO_4$
$Bi_2Sr_2CaCu_2O_8$
T (K)
350
300
250
200
150
100
50
0
T_N
T^*
pseudogap
T_c
SC
AF
pseudogap (spin density wave)
0.2
0.1
0
0.1
0.2
0.3
n
p
0.15
0.15

HTSC Theory

- P. W. Anderson at Princeton University came up with the first theoretical description of these materials, using the resonating valence bond theory, but a full understanding of these materials is still developing today.
- These superconductors are now known to possess a *d*-wave pair symmetry.
- The first proposal that high-temperature cuprate superconductivity involves d-wave pairing was made

  --in 1987 by Bickers, Scalapino and Scalettar

  --in 1988 by theories by Inui, Doniach, Hirschfeld and Ruckenstein, using spin-fluctuation theory,

  -- by Gros, Poilblanc, Rice and Zhang, and by Kotliar and Liu identifying d-wave pairing as a natural consequence of the RVB theory.
- The confirmation of **the d-wave nature** of the cuprate superconductors was made by a variety of experiments, including the direct observation of the d-wave nodes in the excitation spectrum through

  --Angle Resolved Photoemission Spectroscopy

  --the observation of a half-integer flux in tunneling experiments

  --indirectly from the temperature dependence of the penetration depth, specific heat and thermal conductivity.

Resonant Valence Bond (RVB) Theory

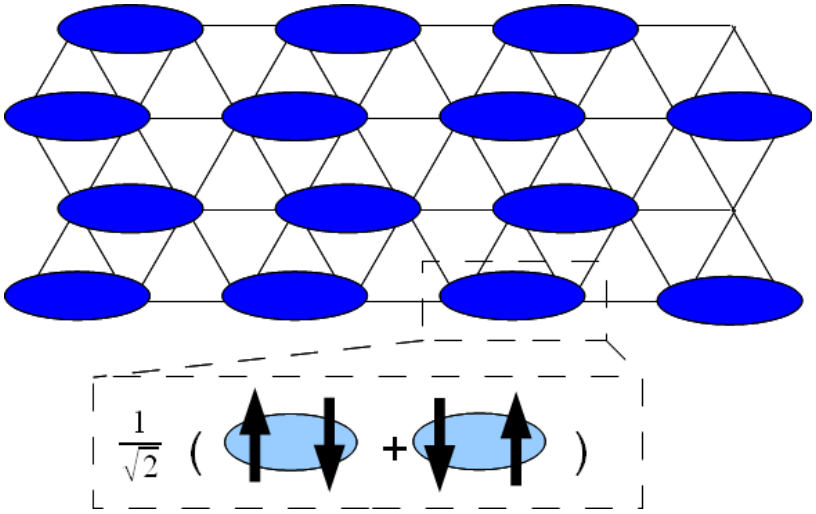

The RVB state with valence bond coupling of nearest-neighbor electrons

- The resonating valence bond theory (RVB) is a theoretical model that attempts to describe high temperature superconductivity, and in particular the superconductivity in cuprate compounds. It was first proposed by P. W. Anderson and G. Baskaran in 1987.
- The theory states that in copper oxide lattices, electrons from neighboring copper atoms interact to form a valence bond, which locks them in place. With doping, these electrons can act as mobile Cooper pairs and are able to superconduct.
- Anderson observed that the origins of superconductivity in doped cuprates was in the Mott insulator nature of crystalline copper oxide. RVB builds on **the Hubbard and t-J models** used in the study of strongly correlated materials.

The Hubbard model

- The Hubbard model is based on the tight-binding approximation from solid state physics. In the tight-binding approximation, electrons are viewed as occupying the standard orbitals of their constituent atoms, and then 'hopping' between atoms during conduction. Mathematically, this is represented as a 'hopping integral' or 'transfer integral' between neighboring atoms, which can be viewed as the physical principle that creates electron bands in crystalline materials, due to overlapping between atomic orbitals. The width of the band depends upon the overlapping amplitude.

- However, the more general band theories **do not consider interactions between electrons explicitly. They consider the interaction of a single electron with the potential of nuclei and other electrons in an average way only**. By formulating conduction in terms of the hopping integral, however, the Hubbard model is able to include the so-called 'onsite repulsion', which stems from the Coulomb repulsion between electrons at the same atomic orbitals.

- This sets up a competition between the hopping integral, which is a function of the distance and angles between neighboring atoms, and the on-site Coulomb repulsion, which is not considered in the usual band theories. The Hubbard model can therefore explain the transition from metal to insulator in certain transition metal oxides as they are heated by the increase in nearest neighbor spacing, which reduces the 'hopping integral' to the point where the onsite potential is dominant.

Now, consider a 1D chain of hydrogen atoms

In second quantization notation, the **Hubbard Hamiltonian** then takes the form:

$$H = -t \sum_{\langle i,j \rangle, \sigma} (c_{i,\sigma}^{\dagger} c_{j,\sigma} + c_{j,\sigma}^{\dagger} c_{i,\sigma}) + U \sum_{i=1}^{N} n_{i\uparrow} n_{i\downarrow},$$

where represents nearest-neighbor interaction on the lattice.

The t-J model was first derived in 1977 from the Hubbard model by Józef Spałek. The model describes strongly correlated electron systems. It is used to calculate high temperature superconductivity states in doped antiferromagnets.

The t-J Hamiltonian is:

$$\hat{H} = -t \sum_{<ij>\sigma} \left(\hat{a}^{\dagger}_{i\sigma} \hat{a}_{j\sigma} + \hat{a}^{\dagger}_{j\sigma} \hat{a}_{i\sigma} \right) + J \sum_{<ij>} \left(\vec{S}_i \cdot \vec{S}_j - n_i n_j / 4 \right)$$

where

- sum over nearest-neighbor sites i and j,
- fermionic creation and annihilation operators,
- spin polarization,

t - hopping integral

$$J = 4t^2/U$$

J - coupling constant ,

U - coulomb repulsion,

- particle number at the site i, and
- spins on the sites i and j.

Superconducting tunneling into high temperature superconductors of $YBa_2Cu_3O_7$ crystals and films (90K)

Break-junction Tunneling on HTSC ceramics (1987)

PHYSICAL REVIEW B VOLUME 35, NUMBER 16 1 JUNE 1987

Break-junction tunneling measurements of the high-T_c superconductor $Y_1Ba_2Cu_3O_{9-\delta}$

J. Moreland, J. W. Ekin, L. F. Goodrich, T. E. Capobianco, and A. F. Clark
Electromagnetic Technology Divison, National Bureau of Standards, Boulder, Colorado 80303

J. Kwo, M. Hong, and S. H. Liou
AT&T Bell Laboratories, Murray Hill, New Jersey 07974
(Received 25 March 1987; revised manuscript received 7 May 1987)

Current-voltage tunneling characteristics in a high-critical-temperature superconducting material containing predominately $Y_1Ba_2Cu_3O_{9-\delta}$ have been measured using the break-junction technique. Sharp gap structure was observed, with the largest superconductive energy gap measured to be $\Delta = 19.5 \pm 1$ meV, assuming a superconductor-insulator-superconductor junction. This energy gap corresponds to $2\Delta/k_BT_c = 4.8$ at $T = 4$ K, for a critical temperature of 93 K (midpoint of the resistive transition).

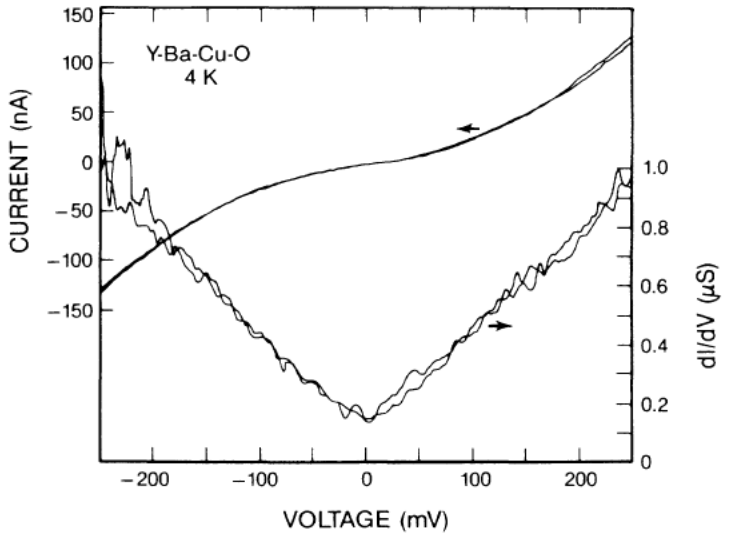

FIG. 1. Current-voltage characteristic and dynamic conductance (dI/dV) characteristic of a $Y_1Ba_2Cu_3O_{9-\delta}$ break junction immersed in liquid helium. This trace is typical of that predominately seen in the sample.

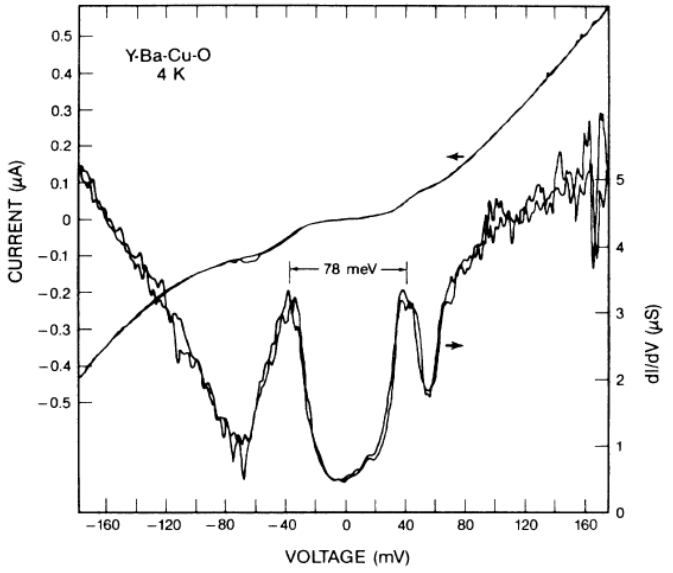

FIG. 2. Current-voltage characteristic and dynamic conductance (dI/dV) showing superconducting gap structure typical of the largest measured in the $Y_1Ba_2Cu_3O_{9-\delta}$ break-junction sample.

Reproducible Tunneling Data on Chemically Etched Single Crystals of $YBa_2Cu_3O_7$

M. Gurvitch, J. M. Valles, Jr., A. M. Cucolo,[a] R. C. Dynes, J. P. Garno, L. F. Schneemeyer, and J. V. Waszczak

AT&T Bell Laboratories, Murray Hill, New Jersey 07974

(Received 26 May 1989)

We have fabricated tunnel junctions between chemically etched single crystals of $YBa_2Cu_3O_7$ and evaporated metal counterelectrodes which exhibit reproducible characteristics. Above the bulk critical temperature of $YBa_2Cu_3O_7$, T_c, the conductance, $G(V)$, has a linear dependence with voltage and has some asymmetry. Below T_c, additional structure associated with the superconductivity appears in $G(V)$. At $T \ll T_c$ there is a reproducible, finite, zero-bias conductance which suggests that there are states at the Fermi energy in superconducting $YBa_2Cu_3O_7$. Junctions with Pb, Sn, Bi, Sb, PbBi, and Au counterelectrodes all show qualitatively similar behavior.

PACS numbers: 74.50.+r, 74.65.+n

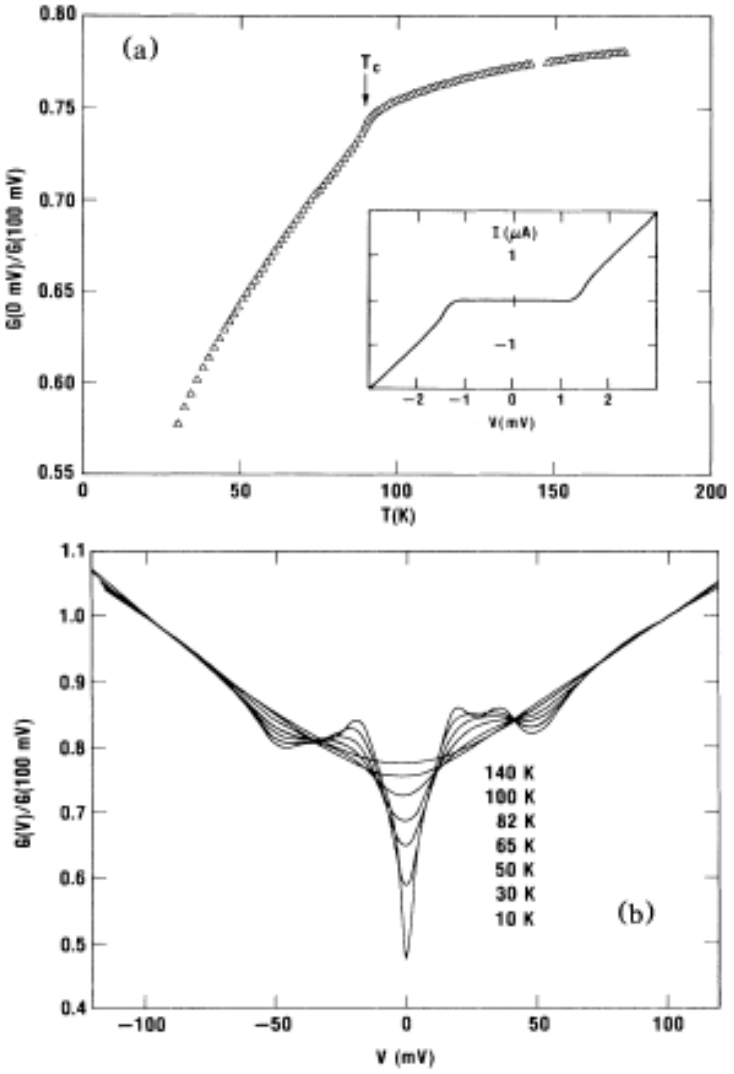

FIG. 1. (a) Temperature dependence of $G(0\ \text{mV})/G(100\ \text{mV})$ of a $YBa_2Cu_3O_7$/Pb junction. Inset: Current vs voltage for a typical junction for $T < 1$ K. Note the absence of leakage. (b) Voltage dependence of $G(V)/G(100\ \text{mV})$ for the temperatures indicated for the junction in (a). The lowest-temperature curve has the lowest zero-bias conductance. The polarity refers to the $YBa_2Cu_3O_7$ electrode.

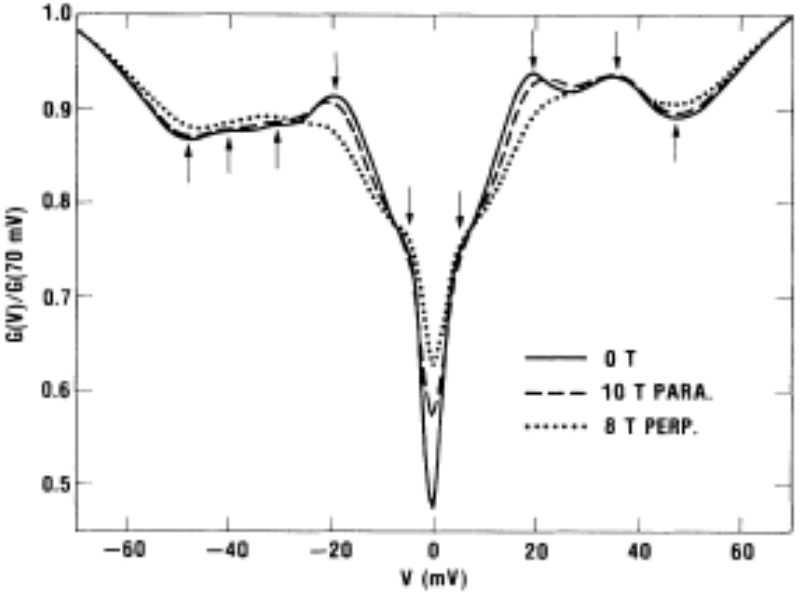

FIG. 2. $G(V)$ for $YBa_2Cu_3O_7$/Pb junction in 0 T (solid line), 10.0 T (dashed line), and 8.0 T (dotted line) magnetic fields at $T = 10$ K. Arrows indicate features which are discussed in the text.

Observations of quasi-particle tunneling and Josephson behavior in $Y_1Ba_2Cu_3O_{7-x}$/native barrier/Pb thin-film junctions

J. Kwo, T. A. Fulton, M. Hong, and P. L. Gammel
AT&T Bell Laboratories, Murray Hill, New Jersey 07974

(Received 4 December 1989; accepted for publication 20 December 1989)

Low-leakage, thin-film planar tunnel junctions made of $Y_1Ba_2Cu_3O_{7-x}$/native barrier/Pb were fabricated. The $Y_1Ba_2Cu_3O_{7-x}$ films were prepared by *in situ* molecular beam epitaxy aided with an activated oxygen source. The as-grown, smooth superconducting perovskite film surface exhibits quasi-particle tunneling characteristics very similar to the etched bulk single-crystal data. The results in agreement are a linear dependence of the normal-state conductance on voltage, a gap-like structure at $\sim$20 mV, asymmetric modulations up to 50 mV, and a finite zero-bias conductance at low temperature. Junctions of lower resistance show, at temperatures below T_c of Pb, the development of a supercurrent at zero bias and associated hysteretic subgap structure, with a typical $I_cR \sim 0.5$ mV. Josephson-like behavior occurred in response to applied magnetic field and microwaves.

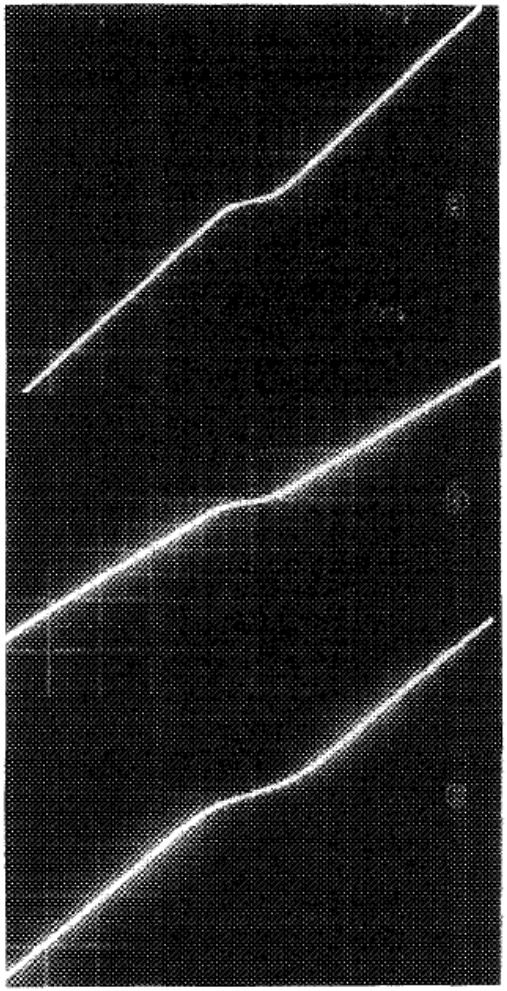

FIG. 1. Current-voltage characteristics for junctions (a), (b), and (c) at 4.2 K. The x axis (voltage) scales are 2, 2, and 1 mV per large division (pld) for (a), (b), and (c), respectively. The y axis (current) scales are 100, 250, and 250 μA pld for (a), (b), and (c), respectively.

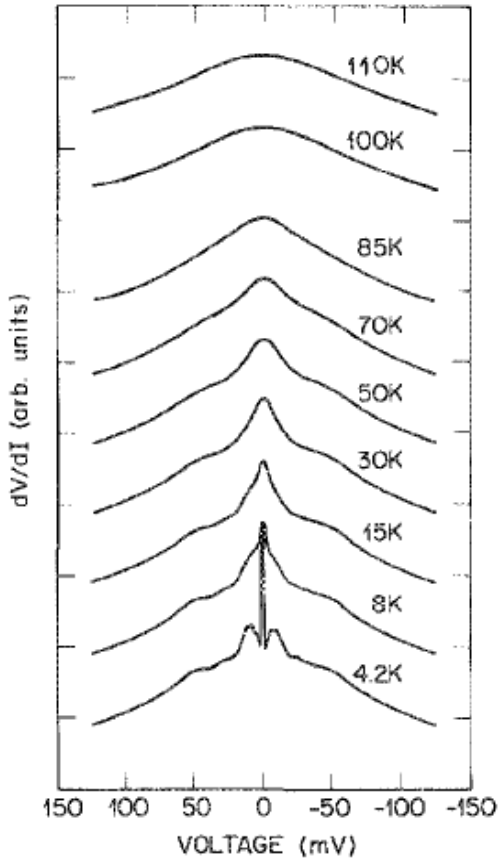

FIG. 2. Dynamic resistance $R(V)$ vs V as a function of temperature below and above T_c of a $Y_1Ba_2Cu_3O_{7-x}$ film. The zero of $R(V)$ at 4.2 K is on the base line, and the zeros of other traces are displaced progressively by one division.

Josephson current

1. Single slit diffraction pattern under B field
2. Shapiro steps in AC microwaves

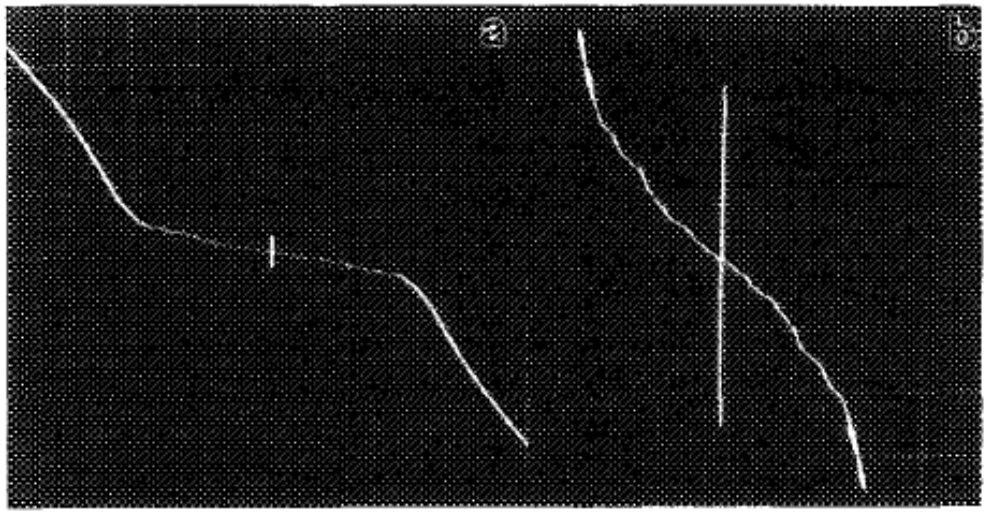

FIG. 3. Supercurrent and assoicated subgap structure at 1.5 K of a junction of R(10 mV) of 80 Ω. The x axis scale is 0.5 mV pld for (a) and (b). The y axis is (a) 10 μA pld and (b) 2 μA pld.

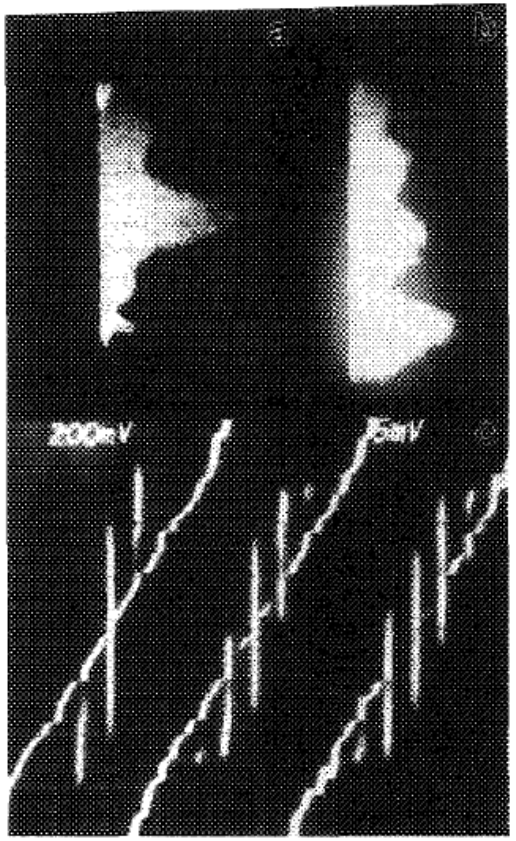

FIG. 4. Critical current (x axis, 1 μA pld) vs applied magnetic field (y axis, 1.9 G pld) for B swept (a) from negative to positive values and (b) in the opposite sense. The junction is in the $V = 0$ state where the trace is bright. (c) Occurrence of Shapiro current steps in the I-V in response to applied microwaves of 11.9 GHz. X scale is 50 μV pld and Y scale is 0.2 μA pld. Applied power is zero, intermediate, and full from left to right. The sloping steps on the leftmost trace are geometrical resonances. Shapiro steps up to $n = 2$ are visible in the right trace.

Iron pnictide superconductors

Iron-based superconductors

- Iron-based superconductors contain layers of iron and a pnictogen—such as arsenic, or phosphorus—or a chalcogen.
- This is currently the family with the second highest critical temperature, behind the cuprates.
- Interest in their superconducting properties began in 2006 with the discovery of superconductivity in LaFePO at 4 K, and gained much greater attention in 2008 after the analogous material LaFeAs(O,F) was found to superconduct at up to 43 K under pressure.
- Simplified doping dependent phase diagrams of iron-based superconductors for both Ln-1111 and Ba-122 materials. The phases shown are the antiferromagnetic/spin density wave (AF/SDW) phase close to zero doping and the superconducting phase around optimal doping.
- The Ln-1111 phase diagrams for La and Sm were determined using muon spin spectroscopy, the phase diagram for Ce was determined using neutron diffraction.

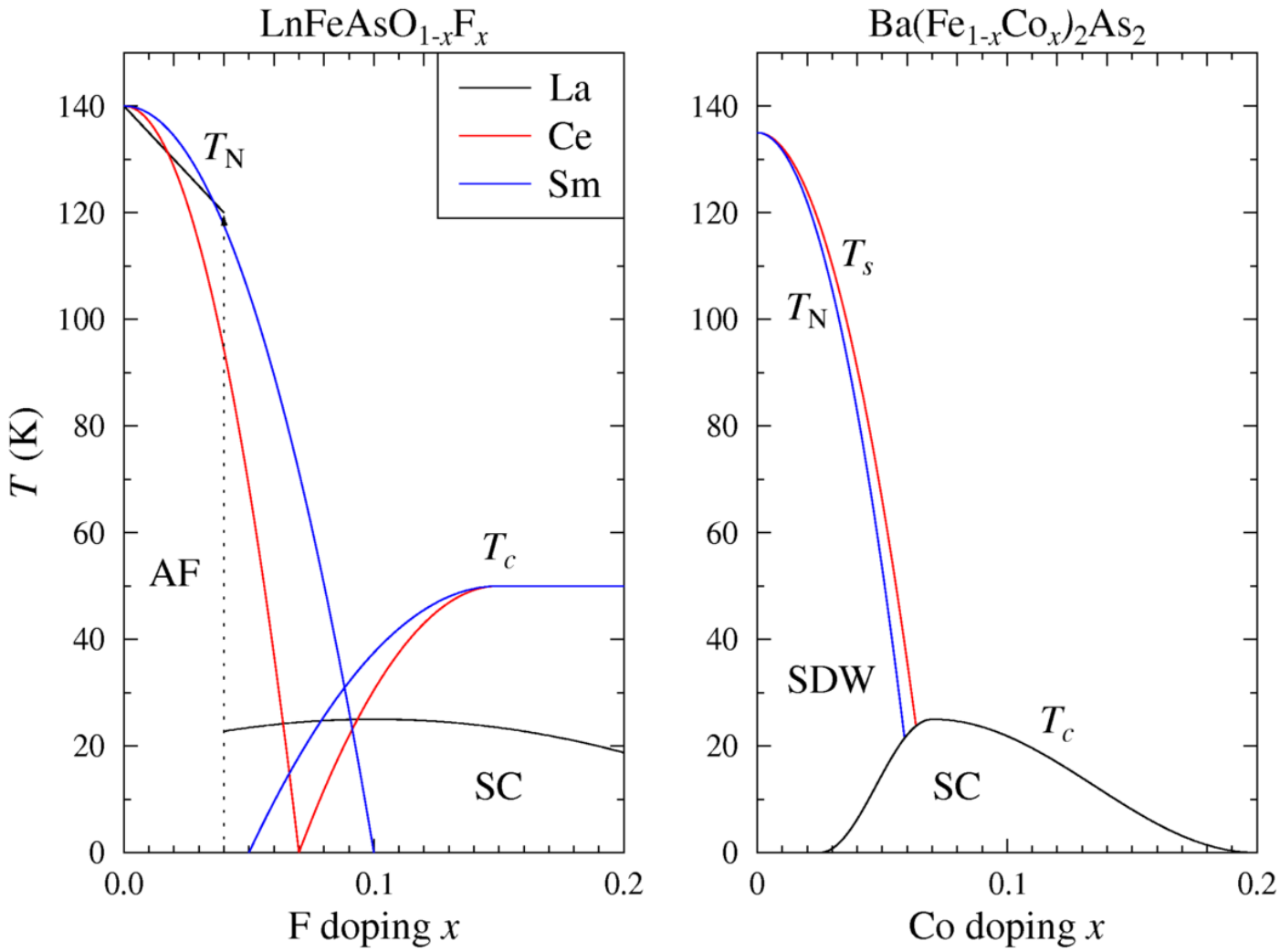
LnFeAsO1-xFx
La
Ce
Sm
TN
Tc
AF
SC
T (K)
F doping x
Ba(Fe1-xCox)2As2
Ts
TN
SDW
Tc
SC
Co doping x

Several families of iron-based superconductors have emerged:

- LnFeAs(O,F) or LnFeAsO1-x with T_c up to 56 K, referred to as 1111 materials.
- A fluoride variant of these materials was subsequently found with similar T_c values.
- (Ba,K)Fe2As2 and related materials with pairs of iron-arsenide layers, referred to as 122 compounds. T_c values range up to 38 K.
- These materials also superconduct when iron is replaced with cobalt LiFeAs and NaFeAs with Tc up to around 20 K. These materials superconduct close to stoichiometric composition and are referred to as 111 compounds.
- FeSe with small off-stoichiometry or tellurium doping.
- Most undoped iron-based superconductors show a tetragonal-orthorhombic structural phase transition followed at lower temperature by magnetic ordering, similar to the cuprate superconductors.
- However, they are poor metals rather than Mott insulators and have five bands at the Fermi surface rather than one.
- The phase diagram emerging as the iron-arsenide layers are doped is remarkably similar, with the superconducting phase close to or overlapping the magnetic phase.
- Strong evidence that the T_c value varies with the As-Fe-As bond angles has already emerged and shows that the optimal Tc value is obtained with undistorted $FeAs_4$ tetrahedral.
- The symmetry of the pairing wave function is still widely debated, but an extended s-wave scenario is currently favored.

Historical development of superconductors

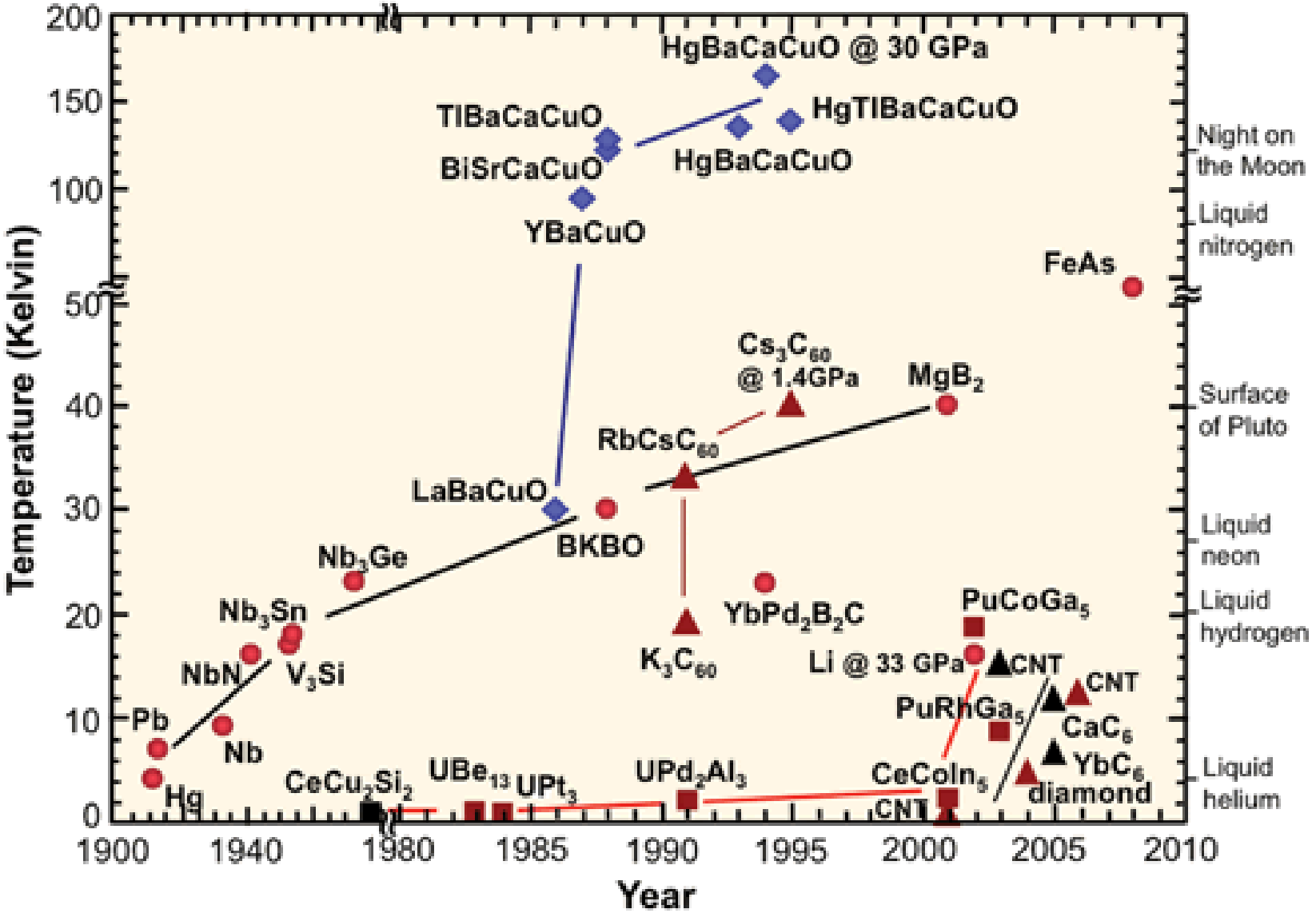

Other materials sometimes referred to as high-temperature superconductors

- Magnesium diboride is occasionally referred to as a high-temperature superconductor, because its T_c value of 39 K is above that historically expected for BCS superconductors. However, it is more generally regarded as the highest Tc conventional superconductor, the increased T_c resulting from two separate bands being present at the Fermi level.

- Fulleride superconductors where alkali-metal atoms (Cs, Rb) are intercalated into C60 molecules show superconductivity at temperatures of up to 38 K for Cs_3C60.

- Some organic superconductors and heavy fermion compounds are considered to be high-temperature superconductors because of their high T_c values relative to their Fermi energy, despite the T_c values being lower than for many conventional superconductors. This description may relate better to common aspects of the superconducting mechanism than the superconducting properties.

- In 1964, William A. Little proposed the possibility of high temperature superconductivity in organic polymers. This proposal is based on the exciton-mediated electron pairing, as opposed to phonon-mediated pairing in BCS theory

- Theoretical work by Neil Ashcroft in 1968 predicted that solid metallic hydrogen at extremely high pressure should become superconducting at approximately room-temperature because of its extremely high speed of sound and expected strong coupling between the conduction electrons and the lattice vibrations. This prediction is yet to be experimentally verified, as the pressure to achieve metallic hydrogen is not known but may be of the order of 500 Gpa.

Critical Fields and Critical Currents

High T_c suggests a high stabilization energy and high energy gap for the superconducting state, from which follow high H_c (from Eq. (9)) and short coherence lengths ξ_0 (from Eq. (17)).

these results lead to extreme type II behavior; high κ in Eq. (37b) and very high H_{c2} . At the high temperatures , thermally activated creep of fluxons may limit useable current values;

1. In the low temperature limit the London penetration depths are $\lambda_{ab} \approx 140$ $\lambda_c \approx 700$ nm,
2. $\xi_{ab} \approx 1.5$ nm , $\kappa_{ab} = \lambda_{ab}/\xi_{ab} \approx 100$, $\xi_c \approx 0.2 - 0.6$ nm,
3. $j_{ab} = 1.2 \times 10^7$ A/cm^2 in the *ab* plane, and $j_c = 4.2 \times 10^5$ A/cm^2 in the *c* direction, suggestive of a quasi-2D superconductor with planes connected by Josephson tunneling.
4. $H_{c2}(ab) \geq 10^7$ G = 1000 T;

Josephson coupling between CuO_2 planes

In narrow bridges (50 nm) much higher critical current densities have been observed, being limited by the depairing of Cooper pairs. A bridge is narrow if no fluxons form within the volume of the bridge, and the GL parameter ψ may be taken as constant within the bridge. Then (I.10) becomes

$$-\frac{\hbar^2}{2m}\frac{d^2\psi}{dx^2} - \alpha\psi + \beta|\psi|^2\psi = 0\,, \quad (10) \qquad -\alpha + \beta\,|\psi|^2 + \tfrac{1}{2}mv^2 = 0, \qquad (62)$$

where the last term is the kinetic energy of the Cooper pairs, each of mass m. The current density is

$$j = 2e|\psi|^2 v = (2e|\psi|^2/m^{1/2})(2\alpha - 2\beta|\psi|^2)^{1/2}, \qquad (63)$$

which is a maximum with respect to $f = |\psi|^2/|\psi_0|^2$ when $f_c = \sqrt{(2/3)}$. Here ψ_0 is the GL parameter at zero current. Thus the maximum (depairing) current density is

$$j_c = (4/3\sqrt{3})(e\kappa/m\xi)|\psi_0|^2; \qquad (64)$$

the critical depairing velocity $v_c \approx \kappa/m\xi$. For $\lambda \approx 100$ nm and $\xi \approx 1$ nm, we have $j_c \approx 1.3 \times 10^9$ A/cm^2 in good agreement with experiment.

Fullerenes

C_{60}; each molecule has the form of a truncated icosahedron with 20 hexagonal faces and 12 pentagonal faces, like a soccer ball.

C_{60} crystallizes in a face-centered cubic structure,

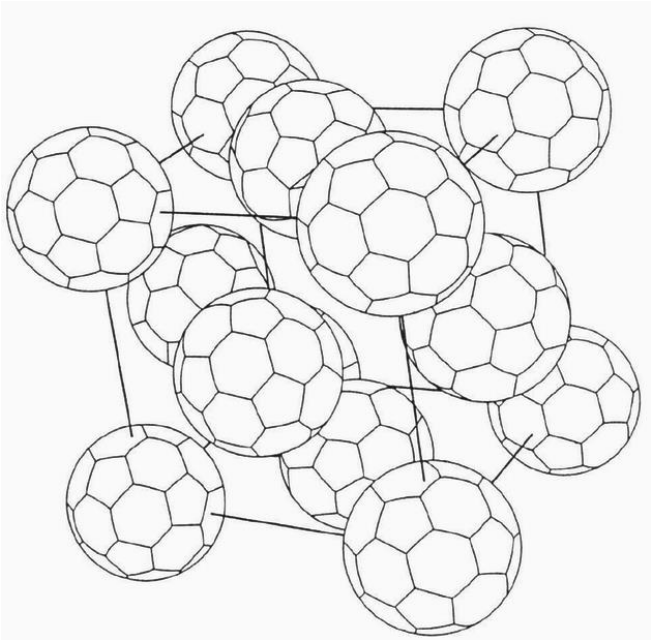

Figure 28 C_{60} fullerene molecules crystallize in a face-centered cubic structure. Courtesy of Steven Louie.

Alkali-fullerene compounds such as K_3C_{60} are superconducting; this one has $T_C = 19.2$ K. The K atoms occupy the octahedral sites in the cubic cell. $RbCs_2C_{60}$ has $T_c = 33$ K.